HHS Public Access

Author manuscript

Mol Cell Endocrinol. Author manuscript; available in PMC 2018 November 05.

Published in final edited form as:

Mol Cell Endocrinol. 2017 November 05; 455: 103–114. doi:10.1016/j.mce.2017.03.019.

Sco2 Deficient Mice Develop Increased Adiposity and Insulin Resistance

Shauna Hill[1,3], **Sathyaseelan S Deepa**[1], **Kavithalakshmi Sataranatarajan**[1], **Pavithra Premkumar**[1], **Daniel Pulliam**[1,3], **Yuhong Liu**[4], **Vanessa Y. Soto**[3], **Kathleen E. Fischer**[4], and **Holly Van Remmen**[1,2,*]

[1]Aging and Metabolism Research Program, Oklahoma Medical Research Foundation, 825 N.E. 13th Street, Oklahoma City, OK, 73104

[2]Oklahoma City VA Medical Center, Oklahoma City, OK

[3]Department of Cellular and Structural Biology, University of Texas Health Science Center at San Antonio, 7703 Floyd Curl Drive, San Antonio, TX 78229

[4]Department of Biology, University of Alabama at Birmingham, 1720 2nd Avenue South, CH 464 Birmingham, AL 35294

Abstract

Cytochrome *c* oxidase (COX) is an essential transmembrane protein complex (Complex IV) in the mitochondrial respiratory electron chain. Mutations in genes responsible for the assembly of COX are associated with Leigh syndrome, cardiomyopathy, spinal muscular atrophy and other fatal metabolic disorders in humans. Previous studies have shown that mice lacking the COX assembly protein Surf1 (*Surf1*$^{-/-}$ mice) paradoxically show a number of beneficial metabolic phenotypes including increased insulin sensitivity, upregulation of mitochondrial biogenesis, induction of stress response pathways and increased lifespan. To determine whether these effects are specific to the *Surf1* mutation or a more general effect of reduced COX activity, we asked whether a different mutation causing reduced COX activity would have similar molecular and physiologic changes. *Sco2 knock-in/knock-out (KI/KO*) mice in which one allele of the *Sco2* gene that encodes a copper chaperone required for COX activity is deleted and the second allele is mutated, have previously been shown to be viable despite a 30–60% reduction in COX activity. In contrast to the *Surf1*$^{-/-}$ mice, we show that *Sco2 KI/KO* mice have increased fat mass, associated with reduced β-oxidation and increased adipogenesis markers, reduced insulin receptor beta (IR-β levels in adipose tissue, reduced muscle glucose transporter 4 (Glut4) levels and a impaired response to the insulin tolerance test consistent with insulin resistance. COX activity and protein are reduced approximately 50% in adipose tissue from the *Sco2 KI/KO* mice. Consistent with the increase in adipose tissue mass, the *Sco2 KI/KO* mice also show increased hepatosteatosis, elevated serum and liver triglyceride and increased serum cholesterol levels compared to wild-type controls. In

*Corresponding author: Holly Van Remmen, PhD, Aging and Metabolism Research Program, Oklahoma Medical Research Foundation, 825 NE 13th Street, Oklahoma City, Oklahoma 73104, Phone: 405-271-2520, Holly-VanRemmen@omrf.org.

contrast to the *Surf1*$^{-/-}$ mice, which show increased mitochondrial number, upregulation of the mitochondrial unfolded protein response (UPR^{MT}) pathway and no significant change in mitochondrial respiration in several tissues, *Sco2 KI/KO* mice do not upregulate the UPR^{MT}, and tissue oxygen consumption and levels of several proteins involved in mitochondrial function are reduced in adipose tissue compared to wild type mice. Thus, the metabolic effects of the *Sco2* and *Surf1*$^{-/-}$ mutations are opposite, despite comparable changes in COX activity, illuminating the complex impact of mitochondrial dysfunction on physiology and pointing to an important role for complex IV in regulating metabolism.

Keywords

Sco2; Complex IV; Adipose Tissue; Insulin Resistance; Mitochondria

1. Introduction

Mitochondria are essential cellular organelles that provide energy to the cell and modulate metabolism through the electron transport chain (ETC) and the process of oxidative phosphorylation. The ETC consists of four mitochondrial transmembrane protein complexes that sequentially transfer electrons from NADH or $FADH_2$ to create an electrochemical proton gradient that provides the energy for ATP production. Complex IV (cytochrome *c* oxidase; COX) performs the final step of oxidative phosphorylation, reducing oxygen to water, to drive the production of ATP. Complex IV consists of 13 subunits, ten of which are encoded by the nuclear genome and assembly of the Complex IV protein is orchestrated by more than 20 different assembly proteins (Saraste, 1990). Mutations in a number of Complex IV subunits have been shown to result in diseases ranging from Leigh's syndrome to hypertrophic cardiomyopathy (Tiranti, Hoertnagel et al. 1998, Shoubridge et al. 2001). For example, mice harboring a musclespecific null mutation in the Complex IV assembly proteins, Cox15 or Cox10, have severe muscle weakness, motor impairment and early deaths (Diaz, Thomas et al. 2005, Viscomi, Bottani et al. 2011). Mice lacking the Complex IV assembly protein Surf1 display only mild muscle weakness and show no motor impairment and paradoxically show an increase in lifespan (Dell'agnello, Leo et al. 2007). Furthermore, studies from our laboratory have shown that in male *Surf1*$^{-/-}$ mice with a 50–70% reduction in COX activity show improved memory, decreased adiposity, enhanced insulin sensitivity, increased mitochondrial number and upregulation of the UPR^{MT}, a mitochondrial stress response pathway (Deepa, Pulliam et al. 2013, Lin, Pulliam et al. 2013, Pulliam, Deepa et al. 2014).

In this study, we asked whether the metabolic phenotype observed in the *Surf1*$^{-/-}$ mice was conserved in another Complex IV mutant mouse model, the *Sco2 KI/KO* mouse. *Sco2 KI/KO* mutant mice have a mutation in the SCO2 gene, which encodes a copper chaperone required for the insertion of copper into the active site of subunit II of Complex IV (Leary, Sasarman et al. 2009). The KI mutation is a point mutation located in the copper-binding site of Sco2 that results in an approximately 50% reduction of copper bound to Sco2 (Jaksch, Paret et al. 2001). In contrast to Surf1, Sco2 is not essential for complete holoenzyme formation. In *Saccharomyces cerevisiae*, in the absence of Sco2, Complex IV is assembled

but lacks the first electron acceptor, copper (Glerum, Shtanko et al. 1996). It has previously been shown that homozygous deletion of the SCO2 gene leads to an embryonic lethal phenotype (Yang, Brosel et al. 2010). However, a Sco2 KI/KO mouse model (*Sco2 KI/KO* mice) in which one *SCO2* allele is deleted (KO) and one is a mutated *SCO2* allele (KI) show a 20–60 % reduction in complex IV activity with no major abnormalities other than muscle weakness (Yang, Brosel et al. 2010). In the current study we asked whether the phenotypes of enhanced insulin sensitivity and reduced fat mass that occur in *Surf1*$^{-/-}$ mice are recapitulated in the *Sco2 KI/KO* mutant mice. In contrast, we show that *Sco2 KI/KO* mice have increased adiposity, are insulin resistant and exhibit other features consistent with metabolic syndrome including high levels of circulating triglycerides and cholesterol. These two genetic alterations lead to similar reductions in Complex IV activity yet have divergent effects on metabolism, suggesting a key connection between the mitochondrial ETC and metabolism that is only beginning to be illuminated.

2. Materials and Methods

Animals

Sco2 KI/KO mice were generated by and obtained from Eric A. Schon (Columbia University Medical Center, New York, NY). *Sco2 KI/KO* mice were previously shown to have a 20–60% decrease in COX activity in several tissues (Yang, Brosel et al. 2010). All experiments were performed according to the protocols approved by the IACUCs at the University of Texas Health Science Center at San Antonio and the Oklahoma Medical Research Foundation. In this study, male wild type control mice were compared to male *Sco2 KI/KO* mice (3–13 months). Animals were fed an ad-libitum diet and were housed in rooms with a 12 hour light and 12 hour dark cycle. Body composition was determined by quantitative magnetic resonance (QMR) (Echo Medial Systems, Houston, TX, USA). Tissues were harvested from mice exposed to carbon dioxide asphyxiation. In this study, visceral white adipose tissue, subcutaneous white adipose tissue and brown adipose tissue were harvested from the perigonadal, flank, and interscapular regions of the mice, respectively.

Food Consumption

Male mice (7–12 months old) were housed in cages in groups of 3–4. Food given to the mice was pre-weighed out at the beginning of the week and then re-weighed the last day of the week. This was repeated each week over the course of one month. Food consumption was calculated as grams per animal per day.

Respirometry

Oxygen consumption was measured using indirect calorimetry as described in (Deepa, Pulliam et al. 2013). Oxygen consumption (VO_2) and CO_2 production (V_{O2}) was measured using the Multiple Animal Respiratory System (MARS) with combined MAD-1 activity detector (Sable Systems International, Las Vegas, NV, USA). Animals were placed individually in normal live-in cages with their standard food and water for 48 h. Animals were given 24 hours to acclimate to the cages and room, oxygen consumption and carbon dioxide production measures from the subsequent 24 hour light-dark cycle were used in

analysis. Energy expenditure (EE) during the light and dark cycles was calculated using the equation EE (kcal/h/kg) = (3.941*VO_2) + (1.106*VCO_2).

Histology

After euthanizing mice, adipose and liver tissue was collected and immediately put in 10% formalin. The tissue sections were embedded in paraffin and sectioned for hematoxylin and eosin (H&E) staining. To evaluate adipocyte morphology, H&E stained sections were analyzed under a light microscope (Nikon Element software, Nikon Inc., Melville, NY, USA). To evaluate lipid content in liver, Oil Red O staining was performed according to (Mehlem, Hagberg et al. 2013).

Triglyceride Measurement in Liver

Liver triglyceride analysis was performed as described in Wang, Al-Regaiey et al. (2006) with the following modifications. Liver tissues (80mg) were homogenized in chloroform:methanol (2:1, v/v) to extract total lipids. Samples were incubated overnight at 4 °C in borosilicate vials. Six calibration standards were prepared concurrently and contained triglyceride standard (Cayman, USA) in the following amounts: 5, 10, 20, 40, 80 and 160 μg in 2 mL of 2:1 chloroform: methanol. Saturated sodium chloride was added to each sample, one half total volume, and vortexed for 15 seconds at top speed. The samples were spun down at 800 × *g* for 20 minutes and the lower organic phase was transferred to a new borosilicate tube. Chloroform (1 mL) was added to the aqueous layer, vortexed, and spun down at 800 × *g* for 5 minutes and the organic layer was collected. The organic layers were pooled together and concentrated down under a stream of nitrogen gas. Lipids were re-suspended in 500 μl of water, incubated at 37 °C for 30 minutes and triglycerides were quantified using the Triglyceride Colorimetric Assay Kit (Cayman Chemical, Ann Arbor, MI).

Cytochrome c oxidase activity assay

COX activity was measured as described in Tzagoloff, Akai et al. (1975) with the following modifications. The enzymatic activity was measured spectrophotometrically by monitoring the rate of oxidation of cytochrome *c* at an absorbance of 550 nm at 30 °C. The assay buffer contained 10 mM KH_2PO_4, 1 mM EGTA, 250 mM sucrose, 10 mM Tris, pH 7.4 and 40 μM of freshly reduced cytochrome *c* (Lustgarten, Jang et al. 2011). Adipose tissue homogenate (100–200mg) was added to 1.5 mL cuvette containing 1 mL of assay buffer and the change in absorbance was recorded over a period of 30 seconds. A cytochrome *c* oxidase inhibitor (0.5 μmol potassium cyanide, KCN) was added to the reaction mixture and the change in absorbance was recorded for an additional 60 seconds. The rate of oxidation of cytochrome *c* was calculated from the change in absorbance at 550 nm and corrected for the non-enzymatic rate of cytochrome *c* oxidation in KCN. The extinction coefficient of 19.6/mM/cm was used to determine the enzymatic activity.

Measuring oxygen consumption in adipose tissue

Oxygen consumption rate was determined using a Seahorse XF24 analyzer according to previous methodologies with the following modifications (Vernochet, Mourier et al. 2012).

Adipose tissue was immediately harvested after mice were euthanized and cut into ~10 mg pieces, washed, and kept on ice in phosphate buffered saline (PBS). Prior to oxygen consumption measurements, adipose tissue pieces were placed in unbuffered Krebs-Henseleit Modified Buffer containing 2.5 mM glucose in Seahorse XF24 Islet Plate (#101174-100; Seahorse Bioscience, North Billerica MA) at 37°C. Oxygen consumption rates were measured with the Seahorse XF24 Flux Analyzer according to (Vernochet, Mourier et al. 2012); basal Oxygen Consumption Rate (OCR) was measured over the course of 3 cycles (2 minutes mix, 2 minutes wait, 3 minutes measure), injection of pyruvate (final concentration 10 mM) with 3 cycles (3 minutes mix, 3 minutes wait, 2 minutes measure) and an injection of carbonyl cyanide-4-(trifluoromethoxy)phenylhydrazone (FCCP, concentration 20 μM) with 3 loops (3 minutes mix, 3 minutes wait, 2 minutes measure). The basal OCR was determined as the third measurement in the run, pyruvate-stimulated OCR was determined as the highest OCR reading post-injection of pyruvate, and maximal OCR was determined as the highest OCR reading post-injection of FCCP.

Blood and Serum Measurements

Serum triglyceride and cholesterol levels were evaluated using the Triglyceride Colorimetric Assay Kit and Cholesterol Fluorometric Assay Kit (Cayman Chemical, Ann Arbor, MI), respectively. Blood glucose levels were measured using One Touch Glucometer. Insulin levels were measured using the Ultra Sensitive Mouse Insulin ELISA Kit (CrystalChem, Downers Grove, IL)

Glucose and Insulin Tolerance Tests

Insulin tolerance test was performed as follows. Mice were fasted for 6 hours. Prior to insulin injection, baseline blood glucose levels were established by measuring blood from tail vein with the One Touch Glucometer. Mice were injected with insulin (1U/kg body weight) (Novolin, Novo Nordisk Inc.) and blood glucose levels were measured at 30 minute intervals over the course of 1.5 hours. Glucose tolerance test was performed similar to the insulin tolerance test except mice were fasted for 16 hours and injected with 2g glucose/kg body weight.

Western Blots

Tissues were homogenized by hand in homogenization buffer (50 mM HEPES pH 7.6, 150 mM NaCl, 2 mM EDTA, 10% glycerol, 1% IgePal, 1 mM $MgCl_2$, 1 mM $CaCl_2$ and protease inhibitor cocktail) with a glass tissue grinder. Following homogenization, samples were spun down at 14,000 rpm for 15 minutes at 4 °C. The clear supernatant was then transferred to a new tube. Protein concentration was determined using the Bradford Assay. Subsequently, 20 μg of protein was loaded onto a sodium dodecyl sulfate polyacrylamide gel electrophoresis (SDS-PAGE) gel and proteins were transferred onto a polyvinylidene fluoride (PVDF) membrane. Primary antibodies used in this study are the following: Phospho-acetyl CoA carboxylase (P-ACC, Ser 79; Cell signaling technology, Danvers, MA), ACC (Cell signaling technology, Danvers, MA), (IRβ, Cell signaling technology, Danvers, MA), Glut4 (Santa Cruz Biotech, Dallas, TX), COX IV (Cell signaling technology, Danvers, MA), UQCRC1 (Abcam, Cambridge, MA), ATP5B (Abcam,), SDHA (Abcam), ATP6E (Santa Cruz Biotech), COXI (Abcam,), TFAM (Proteintech, Rosemont, IL), MnSOD (Proteintech,xxx),

heat shock protein 60 (Hsp60, Enzo, New York, NY), Lon (gift from Luke Szweda, OMRF), ClpP (Sigma, St. Louis, MO), β-actin (Cell signaling technology) and β-tubulin (Sigma). Secondary antibodies used in this study are the following: anti-mouse (Santa Cruz Biotechnology) and anti-rabbit (Santa Cruz Biotechnology). ECL reagent was added to the membrane and protein bands were visualized using G:BOX Chemi XX6 (Syngene, Frederick, MD). Quantification of proteins were performed using GeneTools software (Syngene, Frederick, MD).

Isolated Mitochondria Assays

Isolation of mitochondria from whole tissue was performed according to previous published methodologies (Mansouri, Muller et al., 2006; Chen, Na et al, 2008; Liang, Ran et al., 2009). Mitochondrial hydrogen peroxide production was measured in isolated mitochondria by the Amplex Red fluorescent assay (Muller, Liu et al, 2004). Mitochondrial ATP production was measured in isolated mitochondrial by the ATP bioluminescent firefly luciferase assay (Mansouri, Muller et al.2006).

Quantitative Real Time PCR

For transcript levels, total RNA was extracted from epigonadal white adipose tissue (eWAT, 50 mg) using Trizol reagent (Invitrogen Life Technologies, Carlsbad, CA, USA) according to the manufacturer's instructions. Subsequently, RNA (1μg) is subjected to reverse transcriptase using Retroscript Reverse Transcription kit (Life Technologies) and the resulting cDNA product is diluted 20-fold. A total of 5ng of cDNA was added to the reaction mixture containing 4μl of Power-up SYBR Green (ThermoFisher, Cat. # A25741) and 5 nmol of each primer. Primers used in this study: CCAAT/enhancer-binding protein alpha (C/EBPα) [forward, CAAGAACAGCAACGAGTACCG; reverse, TCACTGGTCAACTCCAGCAC], peroxisome proliferator-activated receptor-γ2 (PPARγ2) [forward, CGAGGACATCCAAGACAAC; reverse, GTGCTCTGTGACGATCTG], adipocyte protein 2 (aP2) [forward, TAACCCTAGATGGCGGGGCCC; reverse, ACACATTCCACCACCAGCTTGTC], long chain acyl CoA dehydrogenase (LCAD) [forward, CTTGCTTGGCATCAACATCGCAGA; reverse, ATTGGAGTACGCTTGCTCTTCCCA],medium chain acyl CoA dehydrogenase (MCAD) [forward, CTAACCCAGATCCTAAAGTACCCG; reverse, GGTGTCGGCTTCCAAATGA], very long chain acyl CoA dehydrogenase (VLCAD) [forward, GGCCAAGCTGGTGAAACACAAGAA; reverse, ACAGAACCACCACCATGGCATAGA]. For mitochondrial DNA copy number, total DNA was extracted from adipose tissue (50 mg) according to (Vernochet, Mourier et al. 2012). A total of 20 ng of genomic DNA was added to the reaction mixture containing 5 μl of Power-up SYBR Green and 5 nmol of each primer; NADH dehydrogenase 2 (ND2): forward, CCTAT- CACCCTTGCCATCAT; reverse, GAGGCTGTTGCTTGTCT-GAC] to the expression of nuclear target sequence (18S: forward, TAGAGGGACAAGTGGCGTTC; reverse, CGCT- GACCCAGTCAGTGT). For all analyses the C_t values were measured using Applied Biosystems QuantStudio® 6 Flex Real-Time PCR System. Relative mtDNA copy number was determined according to (Nicklas, Brooks et al. 2004). Relative mRNA expression was calculated using $2^{-\Delta\Delta Ct}$ analysis. To calculate ΔC_t, the C_t values for 18S (housekeeping gene) was subtracted from the C_t value of the gene of interest. The $\Delta\Delta C_t$ was

determined by calculating the difference between ΔC_t of experimental group (*Sco2 KI/KO*) and control group (wild-type). Relative mRNA expression is expressed as $2^{-\Delta\Delta Ct}$.

Statistics

The unpaired two-sample student's t-test was used to determine statistical significant differences between Sco2 KI/KO to wild-type littermate controls throughout this study for the exception of the tolerance test. The repeated measures ANOVA was used to analyze response to insulin and glucose between Sco2 KI/KO and wild-type littermate mice.

3. Results

Sco2 KI/KO mice have increased adiposity with no change in total body weight

Our previous study showed that male *Surf1*$^{-/-}$ mice lacking Complex IV assembly protein, Surf1, have decreased body weight and fat mass (Deepa, Pulliam et al. 2013). In contrast to the *Surf1*$^{-/-}$ mice, we found that *Sco2 KI/KO* mice have no change in total body weight (Figure 1A). However, quantitative magnetic resonance (QMR) analysis revealed that *Sco2 KI/KO* mice have a significant increase in fat mass and a decrease in lean mass (Figure 1B–C). *Sco2 KI/KO* mice also have a significant increase in kidney wet weight relative to body weight as compared to wild-type littermate controls (Figure 1E). We found no significant differences in skeletal muscle (gastrocnemious) wet weight (Figure 1E). To further investigate the increase in fat mass in the *Sco2 KI/KO* mice, we asked whether increased adiposity was due to one specific fat depot or a universal increase in several fat depots. We found that the mass of the eWAT and subcutaneous white adipose tissue (sWAT) depots were significantly increased in *Sco2 KI/KO* mice compared to wild-type mice, while brown adipose tissue was not different (Figure 1D). Because total body weight is not significantly different between genotypes, the differences in adipose tissue mass represent a real change in body composition. The changes in body composition cannot be explained by differences in food intake because wild-type and *Sco2 KI/KO* mice consumed the same amount of food (3.62 ± 0.07g/mouse/day for wild-type mice and 3.74 ± 0.15 g/mouse/day for *Sco2 KI/KO* mice). To see if these changes in body composition were due to changes in energy expenditure, we analyzed metabolism using indirect calorimetry. Surprisingly, we found that whole body oxygen consumption normalized to lean mass was increased (Figure 1E).

Sco2 KI/KO mice have enlarged adipocytes and reduced fatty acid oxidation in eWAT

Concurrent with the increase in fat mass, *Sco2 KI/KO* mice have enlarged adipocytes in eWAT as indicated by H&E staining of tissue cross sections (Figure 2A). Interestingly, we found no change in adipocyte size in either subcutaneous or brown adipose tissue, despite the increase in subcutaneous fat mass shown in Figure 1B. These findings suggest that there is an overall increase in the total number of subcutaneous adipocytes in the *Sco2 KI/KO* mice since adipocyte size was unchanged and the overall tissue is heavier (Figure 2A). To determine if these changes are due to enhanced adipogenesis or reduced β-oxidation, we measured the expression of genes involved in β-oxidation (VLCAD, LCAD, and MCAD) and adipogenesis (aP2, C/EBPα, PPAR-γ), and the phosphorylation of ACC (Figure 2B and 2C). ACC catalyzes the synthesis of malonyl-CoA, the substrate for fatty acid synthesis and a regulator of fatty acid oxidation (McGarry, Mannaerts et al. 1977, Abu-Elheiga, Jayakumar

et al. 1995). A reduction in ACC phosphorylation down-regulates fatty acid oxidation and promotes fatty acid synthesis (Wakil and Abu-Elheiga 2009). Our data show that phosphorylation of ACC is reduced by 60% in eWAT from *Sco2 KI/KO* mice consistent with reduced β-oxidation and increased fat mass in eWAT (Figure 2B). Phosphorylation of ACC in sWAT from *Sco2 KI/KO* mice is not different from wild-type tissue. We found increased expression of PPARγ (~3-fold), C/EBPα (~1.4-fold) and aP2 (~3-fold) in eWAT from *Sco2 KI/KO* mice (Figure 2C). PPARγ and C/EBPα are critical transcription factors that regulate adipogenesis and differentiation of mature fat cells. Increased expression of these genes supports the potential for enhanced lipid synthesis and increased adipocyte size in the *Sco2 KI/KO* eWAT. Increased expression of aP2, an adipocyte-selective fatty-acid-binding protein and direct target gene of PPARγ is also consistent with increased adipogenesis in the *Sco2 KI/KO* eWAT (Rosen, Hsu et al. 2002).

Sco2 KI/KO mice show liver hepatosteatosis

An increase in adiposity can be associated with elevated serum lipid levels and hepatosteatosis (Liu, Lu et al. 1990). To determine whether *Sco2 KI/KO* mice have increased incidence of hepatosteatosis, liver cross-sections were stained with Oil Red O, a commonly used a fat soluble dye to stain neutral lipids and triglycerides. We found that Oil Red O staining in *Sco2 KI/KO* mice liver is higher, compared to wild-type littermates, suggesting elevated lipid content in *Sco2 KI/KO* mice liver (Figure 3A). Results from Oil Red O staining were confirmed by measuring total triglycerides in lipid extracts prepared from liver. Liver triglycerides are elevated by 24% in *Sco2 KI/KO* mice–(Figure 3B). In addition, serum triglycerides are elevated by 32% and cholesterol levels are elevated by 30% in serum from *Sco2 KI/KO* mice (Figure 3C).

Reduced Complex IV activity and mitochondrial function in adipose tissue of Sco2 KI/KO mice

To confirm that Complex IV activity is reduced in adipose tissue from *Sco2 KI/KO* mice, we measured Complex IV activity using a spectrophotometric assay to monitor the rate of oxidation of cytochrome *c* in whole tissue homogenates. As expected, Complex IV activity is reduced in both *Sco2 KI/KO* eWAT (50%) (Figure 4A). The Seahorse XF24 Flux Analyzer was utilized to determine whether the reduction in Complex IV activity affects mitochondrial function and tissue oxygen consumption. Small pieces of eWAT and sWAT from freshly euthanized mice were analyzed with Seahorse XF24 Flux Analyzer to measure basal, pyruvate-stimulated and FCCP-stimulated oxygen consumption. Basal respiration, pyruvatestimulated respiration, and maximal (FCCP-stimulated) respiration are significantly reduced in both *Sco2 KI/KO* eWAT. (Figure 4B).

Mitochondrial DNA and electron transport chain complexes are altered in Sco2 KI/KO mice

To determine if the reduced oxygen consumption in adipose tissue from *Sco2 KI/KO* mice is associated with reduced mitochondrial protein expression, we measured protein levels of a number of nuclear and mitochondrial encoded proteins and mtDNA copy number in eWAT from wild-type and *Sco2 KI/KO* mice. Western blot analysis of protein levels revealed reduced levels of a subset of ETC proteins, ATP5B, COX IV and COX I, and reduced levels of mitochondrial transcription factor A, TFAM (Figure 5A). Surprisingly, we found a

significantly greater (1.4-fold) mtDNA copy number in *Sco2 KI/KO* mice compared to wild-type mice despite the reduced expression of ETC proteins (Figure 5B). Our previous studies showed that *Surf1*$^{-/-}$ mice have elevated levels of components of the UPR^{MT} in several tissues, (Pulliam, Deepa et al. 2014). In this study, we were interested to determine if the *Sco2 KI/KO* mice had a similar induction in this response in adipose tissue. In contrast to adipose tissue from the *Surf1*$^{-/-}$ mice, we found that protein expression levels of several components of the UPR^{MT}, Lon, Hsp60 and ClpP in the eWAT of *Sco2 KI/KO* mice did not differ compared to wild-type mice (Figure 5C).

Mitochondrial ROS generation and ATP production are not altered in Sco2 KI/KO

Deficits in the mitochondrial electron transport chain are associated with increased mitochondrial reactive oxygen species (ROS) generation and reduced ATP production. To determine whether the mutation in the gene encoding for the Complex IV assembly factor, Sco2 would have an effect on mitochondrial ROS generation and ATP production, we measured hydrogen peroxide generation and ATP production in mitochondria isolated from metabolically active tissues (heart, skeletal muscle, and brain). To measure hydrogen peroxide generation we used Amplex Red, a fluorogenic probe that reacts with hydrogen peroxide to produce the fluorescent product, resorufin. Interestingly, hydrogen peroxide generation was similar in *Sco2 KI/KO* mitochondria in that absence (state I respiration) or in the presence of respiratory substrates, glutamate and malate in skeletal muscle and brain mitochondria or pyruvate and malate in heart mitochondria (Figure 6A–C) and was increased to a similar level in response to inhibitors rotenone and antimycin A. We also measured ATP production in isolated mitochondria using the ATP bioluminescent firefly luciferase assay. Surprisingly, we found no changes in mitochondrial ATP production in the *Sco2 KI/KO* mice (Figure 6D).

Sco2 KI/KO mice are insulin resistant

Mitochondrial dysfunction has been associated with insulin resistance and our previous study showed that Complex IV deficient mice, *Surf1*$^{-/-}$ mice show increased insulin sensitivity compared to wild-type mice. To measure insulin sensitivity in the *Sco2 KI/KO* mice we performed the insulin tolerance test. In contrast to our previous findings with the *Surf1*$^{-/-}$ mice, *Sco2 KI/KO* mice are insulin resistant compared to wild-type littermates (Figure 7A). However, we found no differences in glucose clearance based on the glucose tolerance test (Figure 7B). We also found no differences in the circulating fasted insulin levels but an increase in fed insulin levels (Figure 7C). To determine if alterations in the adipose tissue are in part responsible for reduced insulin sensitivity in the *Sco2 KI/KO* mice, we measured protein expression of IRβ in wild-type and *Sco2 KI/KO* mice by western blot analysis. eWAT from *Sco2 KI/KO* mice has a significant reduction in IRβ expression (0.9-fold change) (Figure 7D). Surprisingly, despite being insulin resistant, protein expression of IRβ (Figure 7D) and phosphorylation of ACC (Figure 7F) were not altered in skeletal muscle from the *Sco2 KI/KO* mice. However, consistent with insulin resistance skeletal, muscle Glut4 levels were reduced by 24% in *Sco2 KI/KO* mice, compared to wild type mice (Figure 7E). These results indicate that altered mitochondrial metabolism due to reduced Complex IV activity promotes insulin resistance through a mechanism that involves the down-regulation of IRβ in eWAT and downregulation of Glut4 in skeletal muscle.

4. Discussion

Our previous studies in *Surf1*$^{-/-}$ mice, a mouse model of Complex IV deficiency that also paradoxically shows increased lifespan (Dell'agnello, Leo et al. 2007), revealed a number of unexpected findings, including increased mitochondrial number in several tissues, induction of the UPR^{MT}, reduced fat mass and increased insulin sensitivity with little or no change in mitochondrial function (Deepa, Pulliam et al. 2013, Pulliam, Deepa et al. 2014). Because altered mitochondrial function has been linked to changes in insulin sensitivity and metabolism, the goal of the current study was to determine whether *Sco2* mutant mice, a Complex IV mutant model with a similar reduction in COX activity, also show a metabolic phenotype similar to the *Surf1*$^{-/-}$ mice. Our results show that *Sco2 KI/KO* mice exhibit a stark difference in phenotype from the *Surf1*$^{-/-}$ mice including increased fat mass, reduced expression of mitochondrial ETC complexes, reduced oxygen consumption in adipose tissue and insulin resistance.

One of the most striking phenotypes we observed in the *Sco2 KI/KO* mice is increased adiposity due to increased subcutaneous and epigonadal fat mass. This is in contrast to previous studies in mouse models of mitochondrial deficiencies, which have shown reduced adiposity. For example, two mouse models of deletion of mitochondrial transcription factor A (TFAM) targeted to adipose tissue show reduced adipose tissue mass and resistance to high fat diet (HFD) induced obesity (Vernochet, Mourier et al. 2012, Vernochet, Damilano et al. 2014). Similarly, muscle and liver specific mitochondrial dysfunction induced by deletion of mitochondrial flavoprotein apoptosis inducing factor (AIF) was shown to result in resistance to age- and HFD-induced weight gain and adipocyte hypertrophy (Pospisilik, Knauf et al. 2007). Finally, these findings in the *Sco2 KI/KO* mice counter our previous findings in the *Surf1*$^{-/-}$ mice, which have reduced adipose tissue and adipocyte size (Deepa, Pulliam et al. 2013). Of further interest is the fact that adipose tissue responds in a depot-specific fashion to the Sco2 mutation and the reduction in COX activity. For example, there is a significant increase in adipocyte size in the eWAT that does not occur in the sWAT despite increased mass in both tissues. Although this is an interesting result, it is important to note that adipocyte size is not always reflected by adipose tissue content .

To reconcile the effect of Sco2 deficiency on fat mass and adipocyte size in these two tissues, we asked whether the changes in adipocyte size were due to alterations in fatty acid synthesis or fat utilization through fatty acid oxidation by determining the phosphorylated state of acetyl-CoA carboxylase (P-ACC). The activity of ACC, the first step of fatty acid synthesis, is regulated by AMPK via phosphorylation. ACC becomes inactive in the phosphorylated state leading to increased fatty acid synthesis (McGarry, Mannaerts et al. 1977). Our data show reduced levels of P-ACC in eWAT, suggesting a preference for fatty acid synthesis over fatty acid oxidation and supporting the increase in mass in this fat depot. In contrast, P-ACC levels are unchanged in sWAT, consistent with no change in adipocyte size in this tissue. We also measured the expression of several genes involved in fatty acid oxidation (VLCAD, LCAD and MCAD) and found no difference in expression of these genes in eWAT from wild type versus *Sco2 KI/KO* mice. In contrast, our previous study showed that *Surf1*$^{-/-}$ mice had increased fatty acid oxidation indicated by an increase in P-

ACC and increased expression of VLCAD consistent with the lean phenotype in the *Surf1*$^{-/-}$ mice (Deepa, Pulliam et al. 2013).

To investigate the hypertrophic adipocyte phenotype further, we asked whether adipogenesis is altered in eWAT from *Sco2 KI/KO* mice. The initiation of adipogenesis requires two key transcriptional regulators of adipogenesis, C/EBPα and PPARγ (Rosen, Walkey et al. 2000, Tontonoz and Spiegelman 2008). C/EBPα, a PPARγ regulator, regulates the expression of genes involved in lipid uptake and pre-adipocyte differentiation as well as the expression of fatty acid binding protein 4, also known as aP2 (Rosen, Hsu et al. 2002, Tontonoz, Hu et al. 1994). Previous studies have shown that PPARγ and C/EBPα levels are associated with adipocyte size and adipose tissue weight (Kubota, Terauchi et al. 1999, Bluher, Patti et al. 2004). Consistent with the increase in fat mass and enlarged adipocytes in the *Sco2 KI/KO* mice, C/EBPα, aP2, and PPARγ, are elevated in eWAT from *Sco2* mutant mice. These findings suggest that the hypertrophic adipocyte phenotype observed in eWAT from *Sco2 KI/KO* mice may be in part due to the transcriptional activation of adipogenesis. Another mechanism to consider is the reduction in the rate of lipolysis in Sco2 *KI/KO* eWAT. A reduction in the rate of lipid breakdown (lipolysis) may give rise to the hypoertrophic adipocyte phenotype.

The increased fat deposition in Sco2 mutant mice is not restricted to adipose tissue. *Sco2 KI/KO* mice also have a significant elevation of circulating triglycerides and cholesterol and a striking accumulation of lipids in the liver. These findings suggest that there is an overall tendency for lipid accumulation in the *Sco2 KI/KO* mutant mice. Increased liver lipid content can be caused by increased de novo lipogenesis in liver or by reduced capacity of WAT to store lipids. Fat accumulation does not appear to be impaired in the *Sco2 KI/KO* mice, suggesting a potential role for de novo lipogenesis or some other mechanism in the fat accumulation in the *Sco2 KI/KO* mice. This finding is again distinct from our findings in *Surf1*$^{-/-}$ mice, where we observed reduced levels of triglycerides in liver and circulation (Deepa, Pulliam et al. 2013).

The mitochondrial phenotype is also different between the *Sco2 KI/KO* and *Surf1*$^{-/-}$ mice. *Sco2 KI/KO* mice have been shown to have a universal decrease in Complex IV activity across tissues along with reduced Complex III in selected tissues (Yang, Brosel et al. 2010). Here we report a significant reduction in COX activity in adipose tissue along with reduced expression of a number of ETC subunit proteins and reduced tissue oxygen consumption in the *Sco2 KI/KO* mice. This is in direct contrast to our previous finding that *Surf1*$^{-/-}$ mice exhibit an induction of ETC subunit proteins in several tissues yet no change in mitochondrial respiration (Deepa, Pulliam et al. 2013). Similar to our results in the *Surf1*$^{-/-}$ mice, we found that mitochondrial generation of ROS and production of ATP are not altered in several tissues from the *Sco2 KI/KO* mice, despite the reduction in oxygen consumption and ETC subunits. This suggests that overall the alterations in mitochondrial function in the *Sco2 KI/KO* mice are relatively mild. Interestingly, we found that mitochondrial DNA copy number is significantly elevated in eWAT from *Sco2 KI/KO* mice, despite the reduction in the level of several ETC complex proteins. Other Complex IV mutants, specifically muscle-specific *Cox15*$^{-/-}$ mice and *Surf1*$^{-/-}$ mice, also show an increase in mtDNA copy possibly as a compensatory attempt to enhance mitochondrial biogenesis and improve mitochondrial

function (Viscomi, Bottani et al. 2011, Deepa, Pulliam et al. 2013). Our study in *Surf1*$^{-/-}$ mice showed that the UPR^{MT} was elevated, thus we were interested to know if the *Sco2* mutant mice also showed induction of UPR^{MT} that might suggest a common response to a reduction in cytochrome *c* oxidase activity. We found no evidence of the induction of the UPR^{MT} in *Sco2 KI/KO* mice. We believe the difference in UPR^{MT} response is related to the fact that the *Surf1*$^{-/-}$ mice have an accumulation of unassembled Complex IV subunits that lead to the UPR^{MT} response. On the other hand, the *Sco2* mutant mice form the holoenzyme with a reduced enzymatic activity and do not provide a stimulus for the UPR^{MT}

Mitochondrial dysfunction and systemic lipid dysregulation have been linked to hyperinsulinemia and insulin resistance (Lowell and Shulman 2005, Savage, Peterson et al. 2007). Paradoxically, *Surf1*$^{-/-}$ mice were previously found to have enhanced insulin sensitivity and reduced insulin levels compared to wild-type controls, despite a significant reduction in Complex IV activity (Deepa, Pulliam et al. 2013). In contrast to the *Surf1*$^{-/-}$ mice we find that circulating insulin levels are elevated in fed *Sco2 KI/KO* mice. Elevated levels of insulin can be a precursor to diabetes and insulin resistance (Johnson, Duick et al. 2010). The insulin tolerance test revealed that *Sco2 KI/KO* mice clear glucose at a significantly lower rate in response to insulin compared to wild-type mice. These findings contradict the phenotype of insulin sensitivity reported in other mitochondrial mutants including mice with targeted AIF deletion in either skeletal muscle or liver, a mouse model of skeletal muscle specific ablation of TFAM and the *Surf1*$^{-/-}$ mice (Wredenberg, Freyer et al. 2006, Pospisilik, Knauf et al. 2007, Deepa, Pulliam et al. 2013). In the case of the *Sco2 KI/KO* mice, reduced lipid utilization and increased circulating lipid levels are likely to contribute to the insulin resistance.

Skeletal muscle has been shown to play an essential role in insulin resistance. The fact that *Sco2 KI/KO* mice have reduced lean mass suggested that skeletal muscle maybe a cause of insulin resistance in the mice. Studies have shown that lean mass is positively correlated to insulin sensitivity (Peterson, Dufour et al. 2007; Brochu, Mathieu et al. 2008). Skeletal muscle is the most important site of glucose disposal in the body and insulin resistance is associated with impaired glucose transport to muscle (DeFronzo RA, Jacot E, 1981; Hollenbeck CB, Chen YD, 1984; Pendergrass M, Bertoldo A; 2007). The Glut4 (glucose transporter 4) protein is enriched in skeletal muscle and is responsible for the majority of insulin-stimulated glucose uptake in skeletal muscle (Hansen, Gulve et al. 1995). Muscle specific ablation of Glut4 results in a significant reduction of insulin-stimulated glucose uptake in mice (Kim, Zisman et al. 2001). *Sco2 KI/KO* mice also have reduced levels of Glut4 in skeletal muscle consistent with reduced glucose transport and insulin resistance. These findings support low insulin stimulated blood glucose clearance in *Sco2 KI/KO* mice.

In summary, our findings showed that *Sco2 KI/KO* mice, a second mouse model of Complex IV deficiency, have a distinct metabolic phenotype that diverges from the *Surf1*$^{-/-}$ mice. There are a number of things that could contribute to the divergent phenotype observed in the *Sco2 KI/KO* mice. For instance, *Sco2 KI/KO* mice were previously shown to have reduced Complex III activity in a select number of tissues whereas Complex III activity is unaffected in *Surf1*$^{-/-}$ mice. This difference could contribute to the different mitochondrial phenotype observed between the two mouse models. The lack of compensation for reduced

Complex IV activity via mitochondrial biogenesis and UPR^{MT} in *Sco2 KI/KO* mice could also contribute to a greater mitochondrial deficit and the distinct metabolic phenotype. It is also very important to note that the strain background of both mouse models may also be a contributing factor to the different response in these two models. The *Sco2 KI/KO* mice are maintained on a C57/Bl6 background while the *Surf1*$^{-/-}$ mice are bred on a DBA2, C57/Bl6 mixed background. The generation of diverse phenotypes found in the *Sco2 KI/KO* and *Surf1*$^{-/-}$ mice, both associated with reduced COX activity, brings up unanswered questions on the role of mitochondrial proteins and mitochondrial function in the regulation of metabolism and insulin resistance. Discovery of the link between mitochondria and metabolic regulation will uncover new pathways for controlling diseases of metabolism.

Acknowledgments

This work was supported by an Ellison Medical Foundation Senior Scholar Award to H.V.R. and a Ruth L. Kirschstein National Research Service Award for Individual Predoctoral Fellows (F31AG047764-03) to S.H. We thank Dr. Eric Schon (Columbia University Medical Center, New York, NY) for providing the Sco2 knock-out and knock-in models to us for this project. We also thank Dr. Ann Louise Olson (Oklahoma University Health Sciences Center) for providing the Glut4 antibody, Dr. Luke Szweda (Oklahoma Medical Research Foundation) for providing the Lon antibody, Amanda Jernigan for assistance with the mice sacrifices, and Dr. Carlo Viscomi for advice and comments on the manuscript. Dr. Van Remmen is supported by a Senior Research Career Scientist Award from the Department of Veterans Affairs.

Literature Cited

Abu-Elheiga L, Jayakumar A, Baldini A, Chirala SS, Wakil SJ. Human acetyl-CoA carboxylase: characterization, molecular cloning, and evidence for two isoforms. Proc Natl Acad Sci U S A. 1995; 92:4011–5. [PubMed: 7732023]

Akerman KE, Wikstrom MK. Safranine as a probe of the mitochondrial membrane potential. FEBS Lett. 1976; 68:191–7. [PubMed: 976474]

Bluher M, Patti ME, Gesta S, Kahn BB, Kahn CR. Intrinsic heterogeneity in adipose tissue of fat-specific insulin receptor knock-out mice is associated with differences in patterns of gene expression. J Biol Chem. 2004; 279:31891–901. [PubMed: 15131119]

Brochu M, Mathieu ME, Karelis AD, Doucet E, Lavoie ME, GarreL D, Rabasa-Lhoret R. Contribution of the lean body mass to insulin resistance in postmenopausal women with visceral obesity: a Monet study. Obesity (Silver Spring). 2008; 16:1085–93. [PubMed: 18356851]

Chen L, Na R, Gu M, Salmon AB, Liu Y, Liang H, Qi W, Van Remmen H, Richardson A, Ran Q. Reduction of mitochondrial H2O2 by overexpressing peroxiredoxin 3 improves glucose tolerance in mice. Aging Cell. 2008; 7:866–78. [PubMed: 18778410]

Deepa SS, Pulliam D, Hill S, Shi Y, Walsh ME, Salmon A, Sloane L, Zhang N, Zeviani M, Viscomi C, Musi N, Van Remmen H. Improved insulin sensitivity associated with reduced mitochondrial complex IV assembly and activity. FASEB J. 2013; 27:1371–80. [PubMed: 23241310]

Defronzo RA, Jacot E, Jequier E, Maeder E, Wahren J, Felber JP. The effect of insulin on the disposal of intravenous glucose. Results from indirect calorimetry and hepatic and femoral venous catheterization. Diabetes. 1981; 30:1000–7. [PubMed: 7030826]

Dell'Agnello C, Leo S, Agostino A, Szabadkai G, Tiveron C, Zulian A, Prelle A, Roubertoux P, Rizzuto R, Zeviani M. Increased longevity and refractoriness to Ca(2+)-dependent neurodegeneration in Surf1 knockout mice. Hum Mol Genet. 2007; 16:431–44. [PubMed: 17210671]

Diaz F, Thomas CK, Garcia S, Hernandez D, Moraes CT. Mice lacking COX10 in skeletal muscle recapitulate the phenotype of progressive mitochondrial myopathies associated with cytochrome c oxidase deficiency. Hum Mol Genet. 2005; 14:2737–48. [PubMed: 16103131]

Glerum DM, Shtanko A, Tzagoloff A. SCO1 and SCO2 act as high copy suppressors of a mitochondrial copper recruitment defect in Saccharomyces cerevisiae. J Biol Chem. 1996; 271:20531–5. [PubMed: 8702795]

Hansen PA, Gulve EA, Marshall BA, Gao J, Pessin JE, Holloszy JO, Mueckler M. Skeletal muscle glucose transport and metabolism are enhanced in transgenic mice overexpressing the Glut4 glucose transporter. J Biol Chem. 1995; 270:1679–84. [PubMed: 7829503]

Hollenbeck CB, Chen N, Chen YD, Reaven GM. Relationship between the plasma insulin response to oral glucose and insulin-stimulated glucose utilization in normal subjects. Diabetes. 1984; 33:460–3. [PubMed: 6373455]

Jaksch M, Paret C, Stucka R, Horn N, Muller-Hocker J, Horvath R, Trepesch N, Stecker G, Freisinger P, Thirion C, Muller J, Lunkwitz R, Rodel G, Shoubridge EA, Lochmuller H. Cytochrome c oxidase deficiency due to mutations in SCO2, encoding a mitochondrial copper-binding protein, is rescued by copper in human myoblasts. Hum Mol Genet. 2001; 10:3025–35. [PubMed: 11751685]

Johnson JL, Duick DS, Chui MA, Aldasouqi SA. Identifying prediabetes using fasting insulin levels. Endocr Pract. 2010; 16:47–52. [PubMed: 19789156]

Kim JK, Zisman A, Fillmore JJ, Peroni OD, Kotani K, Perret P, Zong H, Dong J, Kahn CR, Kahn BB, Shulman GI. Glucose toxicity and the development of diabetes in mice with muscle-specific inactivation of GLUT4. J Clin Invest. 2001; 108:153–60. [PubMed: 11435467]

Kubota N, Terauchi Y, Miki H, Tamemoto H, Yamauchi T, Komeda K, Satoh S, Nakano R, Ishii C, Sugiyama T, Eto K, Tsubamoto Y, Okuno A, Murakami K, Sekihara H, Hasegawa G, Naito M, Toyoshima Y, Tanaka S, Shiota K, Kitamura T, Fujita T, Ezaki O, Aizawa S, Kadowaki T, et al. PPAR gamma mediates highfat diet-induced adipocyte hypertrophy and insulin resistance. Mol Cell. 1999; 4:597–609. [PubMed: 10549291]

Leary SC, Sasarman F, Nishimura T, Shoubridge EA. Human SCO2 is required for the synthesis of CO II and as a thiol-disulphide oxidoreductase for SCO1. Hum Mol Genet. 2009; 18:2230–40. [PubMed: 19336478]

Liang H, Ran Q, Jang YC, Holstein D, Lechleiter J, Mcdonald-Marsh T, Musatov A, Song W, Van Remmen H, Richardson A. Glutathione peroxidase 4 differentially regulates the release of apoptogenic proteins from mitochondria. Free Radic Biol Med. 2009; 47:312–20. [PubMed: 19447173]

Lin AL, Pulliam DA, Deepa SS, Halloran JJ, Hussong SA, Burbank RR, Bresnen A, Liu Y, Podlutskaya N, Soundararajan A, Muir E, Duong TQ, Bokov AF, Viscomi C, Zeviani M, Richardson AG, Van Remmen H, Fox PT, Galvan V. Decreased in vitro mitochondrial function is associated with enhanced brain metabolism, blood flow, and memory in Surf1-deficient mice. J Cereb Blood Flow Metab. 2013; 33:1605–11. [PubMed: 23838831]

Lowell BB, Shulman GI. Mitochondrial dysfunction and type 2 diabetes. Science. 2005; 307:384–7. [PubMed: 15662004]

Lustgarten MS, Jang YC, Liu Y, Qi W, Qin Y, Dahia PL, Shi Y, Bhattacharya A, Muller FL, Shimizu T, Shirasawa T, Richardson A, Van Remmen H. MnSOD deficiency results in elevated oxidative stress and decreased mitochondrial function but does not lead to muscle atrophy during aging. Aging Cell. 2011; 10:493–505. [PubMed: 21385310]

Mansouri A, Muller FL, Liu Y, Ng R, Faulkner J, Hamilton M, Richardson A, Huang TT, Epstein CJ, Van Remmen H. Alterations in mitochondrial function, hydrogen peroxide release and oxidative damage in mouse hind-limb skeletal muscle during aging. Mech Ageing Dev. 2006; 127:298–306. [PubMed: 16405961]

Mcgarry JD, Mannaerts GP, Foster DW. A possible role for malonyl-CoA in the regulation of hepatic fatty acid oxidation and ketogenesis. J Clin Invest. 1977; 60:265–70. [PubMed: 874089]

Mehlem A, Hagberg CE, Muhl L, Eriksson U, Falkevall A. Imaging of neutral lipids by oil red O for analyzing the metabolic status in health and disease. Nat Protoc. 2013; 8:1149–54. [PubMed: 23702831]

Muller FL, Liu Y, Van Remmen H. Complex III releases superoxide to both sides of the inner mitochondrial membrane. J Biol Chem. 2004; 279:49064–73. [PubMed: 15317809]

Nicklas JA, Brooks EM, Hunter TC, Single R, Branda RF. Development of a quantitative PCR (TaqMan) assay for relative mitochondrial DNA copy number and the common mitochondrial DNA deletion in the rat. Environ Mol Mutagen. 2004; 44:313–20. [PubMed: 15476199]

Pendergrass M, Bertoldo A, Bonadonna R, Nucci G, Mandarino L, Cobelli C, Defronzo RA. Muscle glucose transport and phosphorylation in type 2 diabetic, obese nondiabetic, and genetically predisposed individuals. Am J Physiol Endocrinol Metab. 2007; 292:E92–100. [PubMed: 16896161]

Petersen KF, Dufour S, Savage DB, Bilz S, Solomon G, Yonemitsu S, Cline GW, Befroy D, Zemany L, Kahn BB, Papademetris X, Rothman DL, Shulman GI. The role of skeletal muscle insulin resistance in the pathogenesis of the metabolic syndrome. Proc Natl Acad Sci U S A. 2007; 104:12587–94. [PubMed: 17640906]

Pospisilik JA, Knauf C, Joza N, Benit P, Orthofer M, Cani PD, Ebersberger I, Nakashima T, Sarao R, Neely G, Esterbauer H, Kozlov A, Kahn CR, Kroemer G, Rustin P, Burcelin R, Penninger JM. Targeted deletion of AIF decreases mitochondrial oxidative phosphorylation and protects from obesity and diabetes. Cell. 2007; 131:476–91. [PubMed: 17981116]

Pulliam DA, Deepa SS, Liu Y, Hill S, Lin AL, Bhattacharya A, Shi Y, Sloane L, Viscomi C, Zeviani M, Van Remmen H. Complex IV-deficient Surf1(−/−) mice initiate mitochondrial stress responses. Biochem J. 2014; 462:359–71. [PubMed: 24911525]

Rosen ED, Hsu CH, Wang X, Sakai S, Freeman MW, Gonzalez FJ, Spiegelman BM. C/Ebpalpha Induces Adipogenesis Through Ppargamma: A Unified Pathway. Genes Dev. 2002; 16:22–6. [PubMed: 11782441]

Rosen ED, Walkey CJ, Puigserver P, Spiegelman BM. Transcriptional regulation of adipogenesis. Genes Dev. 2000; 14:1293–307. [PubMed: 10837022]

Saraste M. Structural features of cytochrome oxidase. Q Rev Biophys. 1990; 23:331–66. [PubMed: 2178268]

Savage DB, Petersen KF, Shulman GI. Disordered lipid metabolism and the pathogenesis of insulin resistance. Physiol Rev. 2007; 87:507–20. [PubMed: 17429039]

Shoubridge EA. Cytochrome c oxidase deficiency. Am J Med Genet. 2001; 106:46–52. [PubMed: 11579424]

Tiranti V, Hoertnagel K, Carrozzo R, Galimberti C, Munaro M, Granatiero M, Zelante L, Gasparini P, Marzella R, Rocchi M, Bayona-Bafaluy MP, Enriquez JA, Uziel G, Bertini E, Dionisi-Vici C, Franco B, Meitinger T, Zeviani M. Mutations of SURF-1 in Leigh disease associated with cytochrome c oxidase deficiency. Am J Hum Genet. 1998; 63:1609–21. [PubMed: 9837813]

Tontonoz P, Hu E, Graves RA, Budavari AI, Spiegelman BM. mPPAR gamma 2: tissue-specific regulator of an adipocyte enhancer. Genes Dev. 1994; 8:1224–34. [PubMed: 7926726]

Tontonoz P, Spiegelman BM. Fat and beyond: the diverse biology of PPARgamma. Annu Rev Biochem. 2008; 77:289–312. [PubMed: 18518822]

Tzagoloff A, Akai A, Needleman RB, Zulch G. Assembly of the mitochondrial membrane system. Cytoplasmic mutants of Saccharomyces cerevisiae with lesions in enzymes of the respiratory chain and in the mitochondrial ATPase. J Biol Chem. 1975; 250:8236–42. [PubMed: 171256]

Viscomi C, Bottani E, Civiletto G, Cerutti R, Moggio M, Fagiolari G, Schon EA, Lamperti C, Zeviani M. In vivo correction of COX deficiency by activation of the AMPK/PGC-1alpha axis. Cell Metab. 2011; 14:80–90. [PubMed: 21723506]

Wakil SJ, Abu-Elheiga LA. Fatty acid metabolism: target for metabolic syndrome. J Lipid Res. 2009; 50(Suppl):S138–43. [PubMed: 19047759]

Wang Z, Al-Regaiey KA, Masternak MM, Bartke A. Adipocytokines and lipid levels in Ames dwarf and calorie-restricted mice. J Gerontol A Biol Sci Med Sci. 2006; 61:323–31. [PubMed: 16611697]

Wredenberg A, Freyer C, Sandstrom ME, Katz A, Wibom R, Westerblad H, Larsson NG. Respiratory chain dysfunction in skeletal muscle does not cause insulin resistance. Biochem Biophys Res Commun. 2006; 350:202–7. [PubMed: 16996481]

Yang H, Brosel S, Acin-Perez R, Slavkovich V, Nishino I, Khan R, Goldberg IJ, Graziano J, Manfredi G, Schon EA. Analysis of mouse models of cytochrome c oxidase deficiency owing to mutations in Sco2. Hum Mol Genet. 2010; 19:170–80. [PubMed: 19837698]

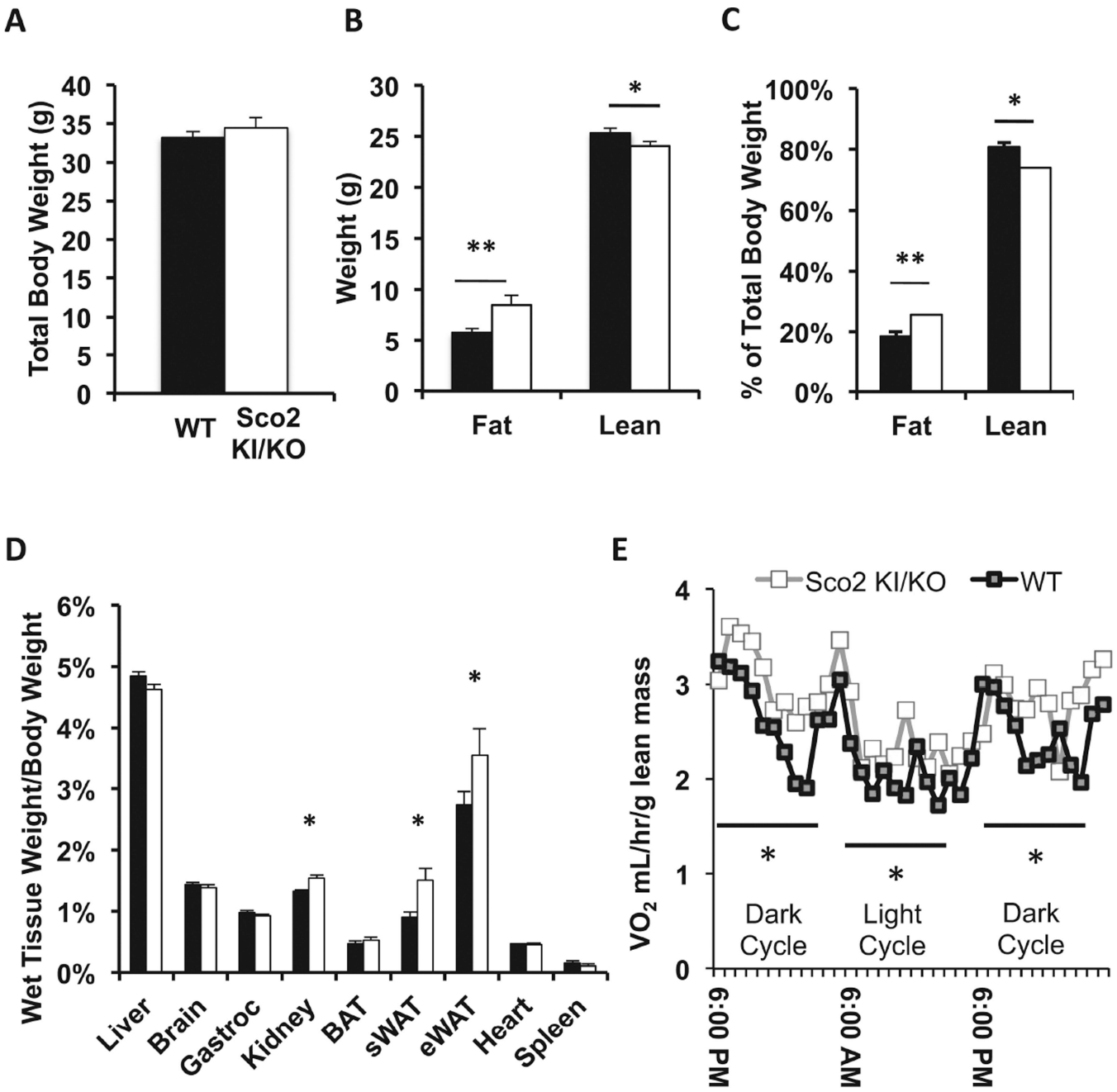

Figure 1. *Sco2 KI/KO* mice have increased adiposity with no change in total body weight

A) Body weight of 10–12 month old male mice (wild-type (WT), n=15; *Sco2 KI/KO*, n=13). Dark bars denote wild-type mice and open bars represent *Sco2 KI/KO* mice. B) Fat mass and lean mass assessed by QMR. C) Percentage of body fat mass and lean mass normalized to body weight. D) Wet tissue weights of 10–12 month old male mice (WT, n=15; *Sco2 KI/KO*, n=13). E) Energy expenditure of 10–12 month old male mice (WT, n=5; *Sco2 KI/KO*, n=6). For all analyses bars depict the mean ± SEM. *Sco2 KI/KO* was compared to the corresponding WT control and statistical significance was determined with the unpaired Student's t-test (**, $p < 0.0025$; *, $p < 0.03$).

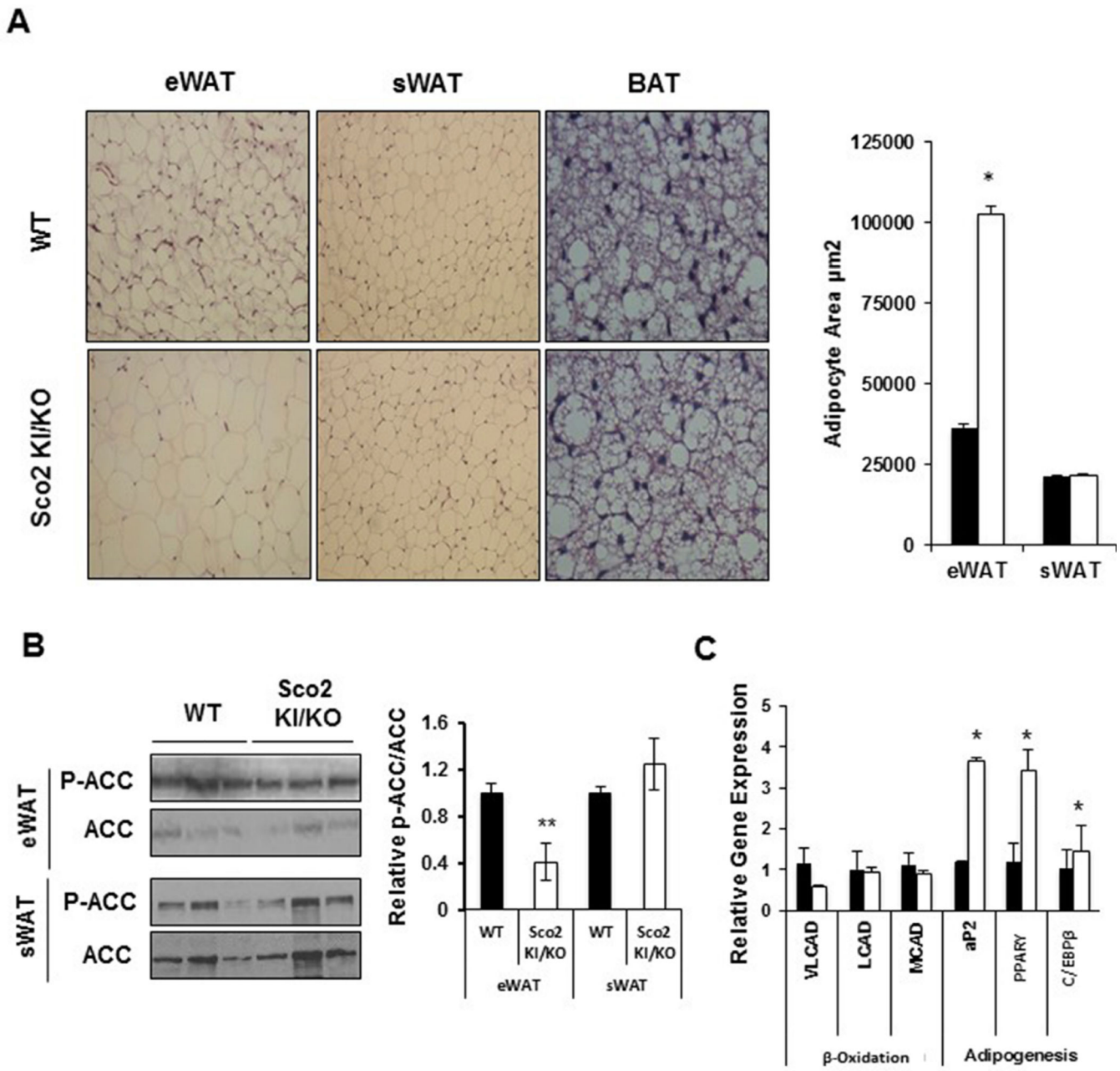

Figure 2. *Sco2 KI/KO* mice have enlarged white epigonadal adipocytes and adipogenesis

A) Representative images of H&E staining of eWAT, sWAT and BAT sections from 10–12 month old male mice (WT, n=6; *Sco2 KI/KO*, n=6); viewed at 20× magnification. B) Area of epigonadal and subcutaneous adipocytes. C) Western blots of P-ACC and ACC in *Sco2 KI/KO* eWAT and sWAT. Levels of P-ACC to ACC is represented graphically in the right panel. D) Relative transcript levels of β-oxidation and adipogenesis related genes in eWAT. The relative values were calculated using ΔΔCt values comparing *Sco2 KI/KO* to the littermate WT control. The bars depict the mean ± SEM and statistical significance between *Sco2 KI/KO* and WT control was determined with the unpaired Student's t-test (*, $p < 0.02$). Dark bars denote wild-type mice and open bars represent *Sco2 KI/KO* mice.

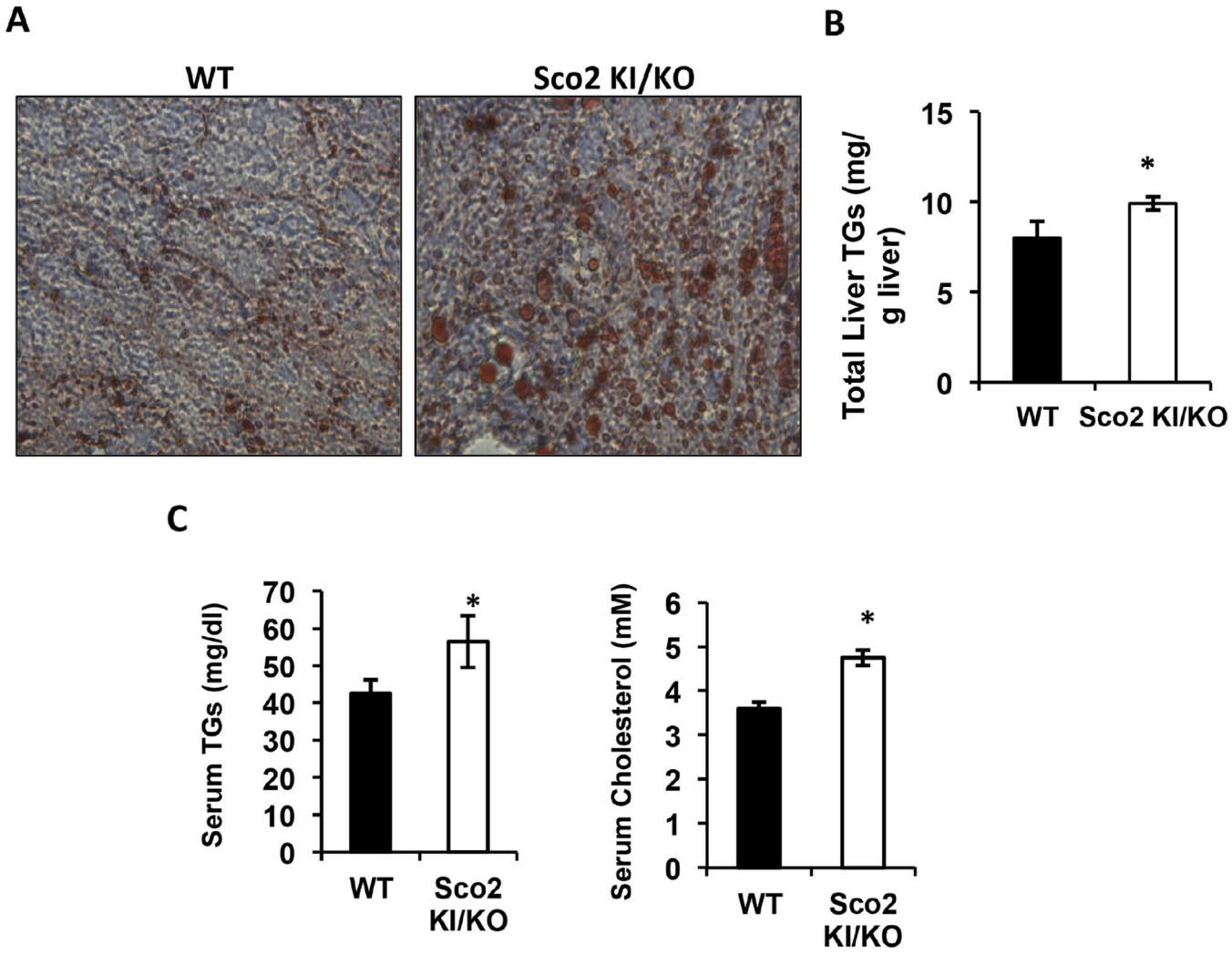

Figure 3. *Sco2 KI/KO* mice have hepatosteatosis

A) Representative images of Oil Red O staining of liver sections from 10–12 month old male mice (WT, n=6; *Sco2 KI/KO*, n=6); viewed at 20× magnification. B) Total liver triglyceride (TG) levels in 10–12 month old male mice. The relative total level of liver triglyceride content of *Sco2 KI/KO* was compared to the corresponding WT control (*, $p < 0.03$). C) The relative circulating triglyceride content in Sco2 KI/KO were compared to WT littermate control (*, $p < 0.043$). D) The relative circulating cholesterol content of *Sco2 KI/KO* were compared to WT littermate control (*, $p < 0.009$). The bars depict the mean ± SEM (WT, n=6; Sco2 KI/KO, n=6) and statistical significance was determined with the unpaired Student's t-test.

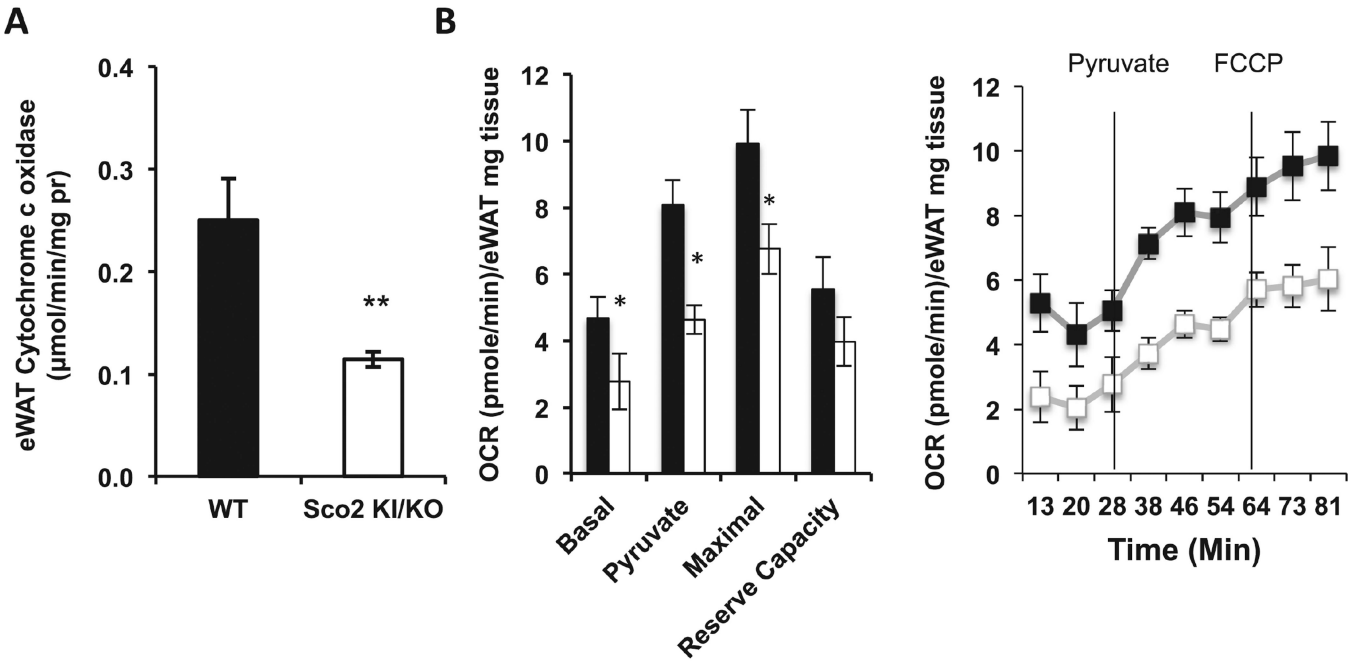

Figure 4. Sco2 mutation alters Complex IV activity and oxygen consumption in adipose tissue

A) COX activity measured in eWAT (left panel) and sWAT (right panel) homogenates. B) OCR of eWAT (left panel) and sWAT (right panel) (~10 mg pieces) was determined using Seahorse XF24 Flux Analyzer under basal, pyruvate, and FCCP-stimulated respiration conditions. The relative OCR of Sco2 KI/KO are compared to the littermate WT control (*, $p < 0.05$; **, $p < 0.001$). For all analyses, the bars depict the mean ± SEM of the OCR of 2–3 tissue pieces/tissue/mice (WT, n=4; *Sco2 KI/KO*, n=4). Dark bars denote wild-type mice and open bars represent *Sco2 KI/KO* mice.

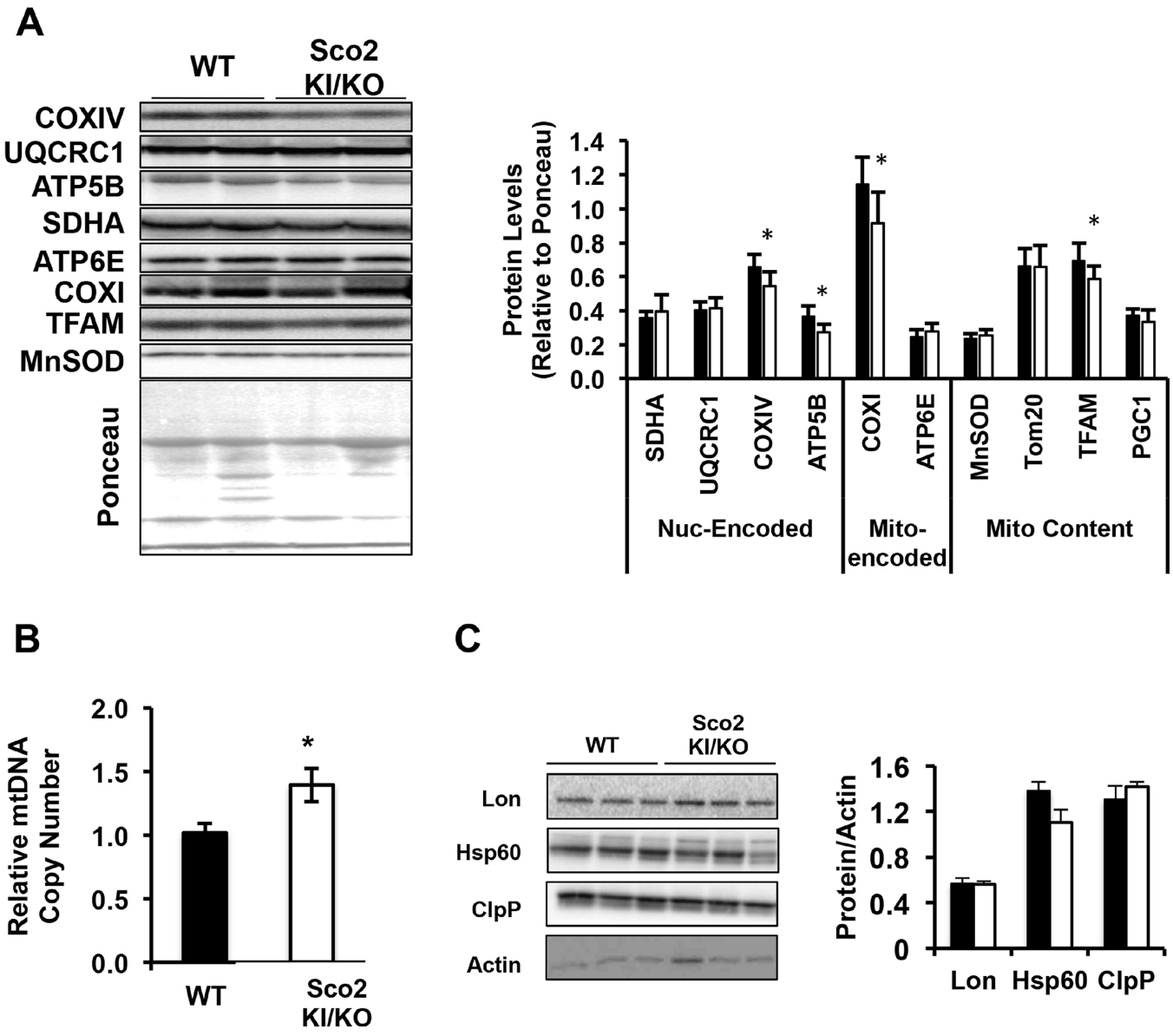

Figure 5. Mitochondrial DNA and ETC complexes are altered in *Sco2 KI/KO* eWAT

A) Western blot analysis of mitochondrial resident proteins and ETC subunits. B) Quantitation of western blots in 5A relative to Ponceau. C) Relative mtDNA copy number in eWAT by quantitative real time PCR (*, $p<0.05$). D) Representative immuno blots of UPR^{MT} components Lon, Hsp60 and ClpP in eWAT. β-actin was used as a loading control. E) Quantitation of immuno blots in 5D relative to Ponceau. For all analyses, the bars depict the mean ± SEM (WT, n=6; *Sco2 KI/KO*, n=6) and statistical significance was determined with the unpaired Student's t-test. Dark bars denote wild-type mice and open bars represent *Sco2 KI/KO* mice.

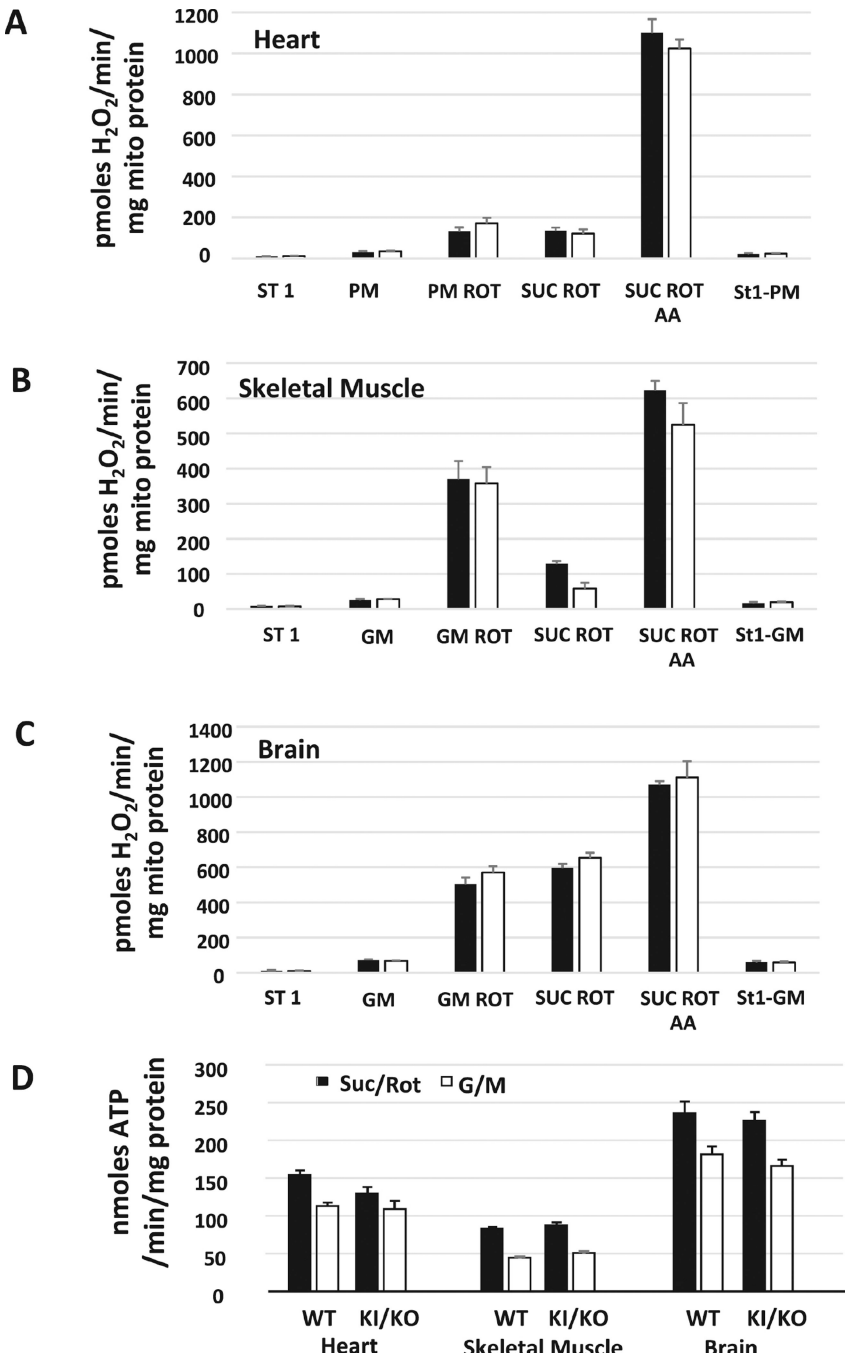

Figure 6. *Sco2 KI/KO* mice do not show increased mitochondrial ROS or compromised production of ATP

(A–C) Mitochondria generation of hydrogen peroxide was measured in isolated mitochondrial from heart, skeletal muscle and brain of 4 to 6 month old wild-type control and *Sco2 KI/KO* mice (n=4–5 mice). Mitochondrial ROS generation was measured using Amplex Red as we have previously described (Muller, Liu et al., 2004). (D) ATP generation was measured using a luciferase based system as previously described (Mansouri, Muller et al., 2006).

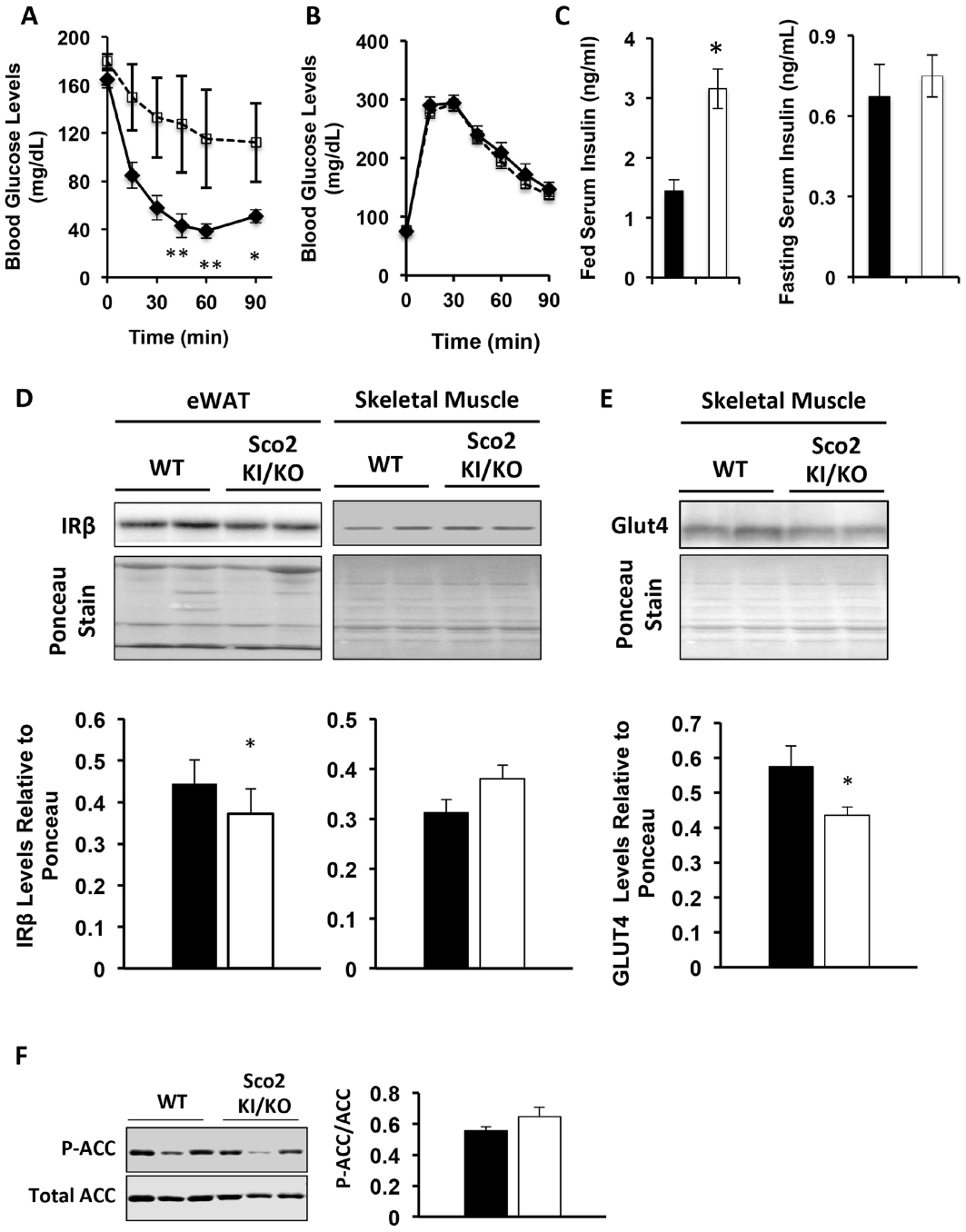

Figure 7. ***Sco2 KI/KO*** **mice are insulin resistant**

A–B) Intraperitoneal insulin (A) and glucose (B) tolerance test was performed in 7–9 month old male mice. C) Circulating insulin levels in 10–12 month old male mice. D) Western blot analysis of insulin-receptor β (IR-β) in eWAT and skeletal muscle. Ponceau staining of the entire membrane was used as a loading control. Quantitation of western blots are shown below the designated blots. E) Western blot analysis of Glut4 in skeletal muscle. Ponceau staining of the entire membrane was used as a loading control. Quantitation of western blots are shown below the designated blot. F) Western blot analysis of P-ACC and ACC in

skeletal muscle. Relative levels of P-ACC normalized to ACC are shown on the right panel. All western blot analysis was performed with tissues from 10–12 month old male mice. The bars depict the mean ± SEM (WT, n=8; *Sco2 KI/KO*, n=8) and statistical significance between *Sco2 KI/KO* and WT control was determined with the unpaired Student's t-test (*, $p < 0.05$). Dark bars denote wild type mice and open bars are Sco2 KI/KO mice.